Experimental Entanglement and Nonlocality of a Two-Photon Six-Qubit Cluster State

Raino Ceccarelli,[1,*] Giuseppe Vallone,[2,1,*] Francesco De Martini,[1,3,*] Paolo Mataloni,[1,*] and Adán Cabello[4]

[1]*Dipartimento di Fisica della "Sapienza" Università di Roma, Roma 00185, Italy and Consorzio Nazionale Interuniversitario per le Scienze Fisiche della Materia, Roma 00185, Italy*

[2]*Centro Studi e Ricerche "Enrico Fermi", via Panisperna 89/A, Compendio del Viminale, Roma 00184, Italy*

[3]*Accademia Nazionale dei Lincei, via della Lungara 10, Roma 00165, Italy*

[4]*Departamento de Física Aplicada II, Universidad de Sevilla, E-41012 Sevilla, Spain*

(Received 4 May 2009; published 13 October 2009)

We create a six-qubit linear cluster state by transforming a two-photon hyperentangled state in which three qubits are encoded in each particle, one in the polarization and two in the linear momentum degrees of freedom. For this state, we demonstrate genuine six-qubit entanglement, persistency of entanglement against the loss of qubits, and higher violation than in previous experiments on Bell inequalities of the Mermin type.

DOI: 10.1103/PhysRevLett.103.160401 PACS numbers: 03.67.Bg, 03.65.Ud, 42.50.Ex, 42.65.Lm

Introduction.—Progress in one-way quantum computing [1] requires the creation of n-qubit graph states [2] of a high number of qubits. Graph states are also fundamental resources for quantum nonlocality [3–6], quantum error correction [7], and quantum entanglement [2,8]. In order to create multiqubit graph states, it is possible to increase the number of entangled particles [9–16] or to encode many qubits in each of them [17–20]. Multiqubit graph states can be created by distributing the qubits between the particles so that each particle carries one qubit. This is the way in which four-qubit graph states with atoms [9] and photons [10–14], and six-qubit graph states with atoms [15] and photons [16] were created. A second strategy is to distribute the qubits so that each of the particles encode two qubits. This has been used to create two-photon four-qubit graph states [17–19] and up to five-photon ten-qubit graph states [20]. By generalizing this strategy, we have created a six-qubit two-photon linear cluster state $|\widetilde{\mathrm{LC}}_6\rangle$, by encoding three qubits in each particle: one qubit in the polarization and two qubits in the linear momentum degrees of freedom (DOFs). The $|\widetilde{\mathrm{LC}}_6\rangle$ is the only distribution of six qubits between two particles whose perfect correlations have the same nonlocality as those of the six-qubit Greenberger-Horne-Zeilinger state [6], but only requires two separated carriers [5].

Consider the graph in Fig. 1 and associate a single qubit to each vertex. The linear cluster state $|\mathrm{LC}_6\rangle$ is defined as the only six-qubit state which satisfies $g_i|\mathrm{LC}_6\rangle = |\mathrm{LC}_6\rangle$, $\forall\ i$, where g_i corresponds to the vertex i of the graph in Fig. 1, and is defined as $g_i = X_i \bigotimes_{j\in\mathcal{N}(i)} Z_j$, where, e.g., X_i is the Pauli matrix σ_x of qubit i, and $\mathcal{N}(i)$ is the set of vertices which are connected to i. An equivalent definition of graph states can be given in terms of controlled-Z operations defined on qubits i and j as $\mathrm{CZ}_{ij} = |0\rangle_i\langle 0| \otimes \mathbb{1}_j + |1\rangle_i\langle 1| \otimes Z_j$. The graph state $|\mathcal{G}\rangle$ associated to the N-vertex graph $\mathcal{G}$ can be written as

$$|\mathcal{G}\rangle = \Big(\prod_{\langle i,j\rangle} \mathrm{CZ}_{ij}\Big) \bigotimes_{i=1}^{N} |+\rangle_i, \tag{1}$$

where $\langle i, j\rangle$ indicates the connected vertices in $\mathcal{G}$ and $|+\rangle_i = \frac{1}{\sqrt{2}}(|0\rangle_i + |1\rangle_i)$.

The specific distribution of the six qubits between the two photons in Fig. 1 (qubits 1, 2, and 3 are carried by photon A, and qubits 4, 5, and 6 by photon B) allows bipartite nonlocality [5] because, in this distribution, all the single-qubit Pauli observables satisfy the EPR criterion for elements of reality [21], since the result of measuring any of the Pauli observables on qubits 1, 2, and 3 can be predicted with certainty from measurements on qubits 4, 5, and 6, and vice versa. This property is not satisfied by other methods of creating graph states using different DOFs of the same photon, where new qubits are added by local operations [20].

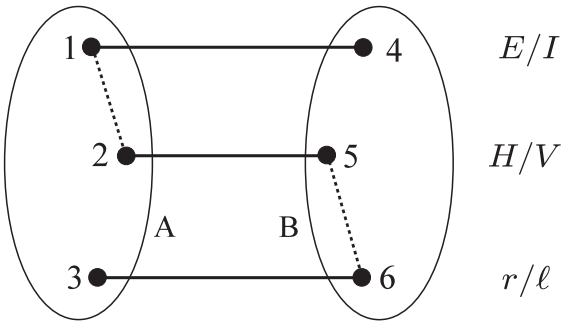

FIG. 1. Graph associated to a two-photon six-qubit entangled state. Each set represents a photon and each vertex corresponds to a qubit. Each link represents a CZ operation between the two connected qubits. Dashed lines represent links present in the $|\mathrm{LC}_6\rangle$ state and absent in the $|\mathrm{HE}_6\rangle$ state. In the experiment, qubits 1 and 4 are encoded into external/internal (E/I) modes, qubits 2 and 5 into horizontal/vertical (H/V) polarization, and qubits 3 and 6 into right/left (r/ℓ) modes. See the text for details.

Experimental preparation.—We create the state $|\widetilde{\mathrm{LC}}_6\rangle$, equivalent up to single-qubit unitary transformations to $|\mathrm{LC}_6\rangle$, in two steps: first, we prepare a six-qubit hyperentangled state ($|\widetilde{\mathrm{HE}}_6\rangle$) (cf. Fig. 1) by a triple entanglement of two photons. The quantum information is encoded in the polarization (qubits 2 and 5) and longitudinal momentum (qubits 1 and 4, and 3 and 6) photon DOFs. Then, we transform $|\widetilde{\mathrm{HE}}_6\rangle$ into $|\widetilde{\mathrm{LC}}_6\rangle$ by applying a sequence of unitary transformations which entangle qubits 1 and 2, and qubits 5 and 6.

The experimental setup used to create and measure the $|\widetilde{\mathrm{LC}}_6\rangle$ is illustrated in Fig. 2. We used spontaneous parametric down conversion in a single 0.5 mm thick Type I β-barium–borate (BBO) crystal excited by a continuous wave UV laser, following a scheme described in Fig. 2 [22,23]. Precisely, four pairs of correlated spatial modes [24], labeled as ℓ (r) for the left (right) side of the emission cone and as I (E) considering the internal (external) modes [cf. Fig. 2(a)] were selected within the conical emission of the crystal. The starting point for the cluster state generation was the six-qubit $|\widetilde{\mathrm{HE}}_6\rangle$, given by the product of one polarization and two longitudinal momentum entangled states,

$$|\widetilde{\mathrm{HE}}_6\rangle = \frac{1}{\sqrt{2}}(|EE\rangle_{AB} + |II\rangle_{AB}) \otimes \frac{1}{\sqrt{2}}(|HH\rangle_{AB} - |VV\rangle_{AB}) \otimes \frac{1}{\sqrt{2}}(|\ell r\rangle_{AB} + |r\ell\rangle_{AB}), \quad (2)$$

where A (B) corresponds to the up (down) side of the conical crystal emission.

By using the following correspondence between physical states and qubit states

$$\{|E\rangle_A, |I\rangle_A\} \rightarrow \{|0\rangle_1, |1\rangle_1\}, \quad (3a)$$
$$\{|H\rangle_A, |V\rangle_A\} \rightarrow \{|0\rangle_2, |1\rangle_2\}, \quad (3b)$$
$$\{|r\rangle_A, |\ell\rangle_A\} \rightarrow \{|0\rangle_3, |1\rangle_3\}, \quad (3c)$$
$$\{|E\rangle_B, |I\rangle_B\} \rightarrow \{|0\rangle_4, |1\rangle_4\}, \quad (3d)$$
$$\{|H\rangle_B, |V\rangle_B\} \rightarrow \{|0\rangle_5, |1\rangle_5\}, \quad (3e)$$
$$\{|r\rangle_B, |\ell\rangle_B\} \rightarrow \{|0\rangle_6, |1\rangle_6\}, \quad (3f)$$

the hyperentangled state (2) is equivalent, up to single-qubit unitary transformations, to the graph state $|\mathrm{HE}_6\rangle$ shown in Fig. 1. Specifically, $|\widetilde{\mathrm{HE}}_6\rangle = H_2X_3H_3H_4Z_5|\mathrm{HE}_6\rangle$, where H_i denotes the Hadamard operation on qubit i. By Eq. (1), the cluster state $|\mathrm{LC}_6\rangle$ is obtained from $|\mathrm{HE}_6\rangle$ by applying the CZ_{12} and CZ_{65} gates. Then, by applying the gates CX_{12} (a controlled-X operation) and CZ_{65} on the hyperentangled state $|\widetilde{\mathrm{HE}}_6\rangle$, we obtain

$$|\widetilde{\mathrm{LC}}_6\rangle = \mathrm{CX}_{12}\mathrm{CZ}_{65}|\widetilde{\mathrm{HE}}_6\rangle = H_2X_3H_3H_4Z_5|\mathrm{LC}_6\rangle. \quad (4)$$

The created state, $|\widetilde{\mathrm{LC}}_6\rangle$, is, up to a unitary transformation, equivalent to the two-photon six-qubit cluster state $|\mathrm{LC}_6\rangle$ by the correspondence (4). Specifically, the relation given in (4) between $|\widetilde{\mathrm{LC}}_6\rangle$ and $|\mathrm{LC}_6\rangle$, implies that $|\widetilde{\mathrm{LC}}_6\rangle$ is the only common eigenstate of the generators $\tilde{g}_i$ obtained from g_i by changing $X_2 \leftrightarrow Z_2$, $X_3 \rightarrow -Z_3$, $Z_3 \rightarrow X_3$, $X_4 \leftrightarrow Z_4$, and $X_5 \rightarrow -X_5$. Qubits 1 and 4 are encoded by the E/I degree of freedom, qubits 2 and 5 by the H/V polarization, and qubits 3 and 6 by the r/ℓ degree of freedom.

The $|\widetilde{\mathrm{LC}}_6\rangle$ state can be written as

$$|\widetilde{\mathrm{LC}}_6\rangle = \frac{1}{2}[|EE\rangle_{AB}|\phi^-\rangle_\pi|\ell r\rangle_{AB} + |EE\rangle_{AB}|\phi^+\rangle_\pi|r\ell\rangle_{AB} - |II\rangle_{AB}|\psi^-\rangle_\pi|\ell r\rangle_{AB} + |II\rangle_{AB}|\psi^+\rangle_\pi|r\ell\rangle_{AB}], \quad (5)$$

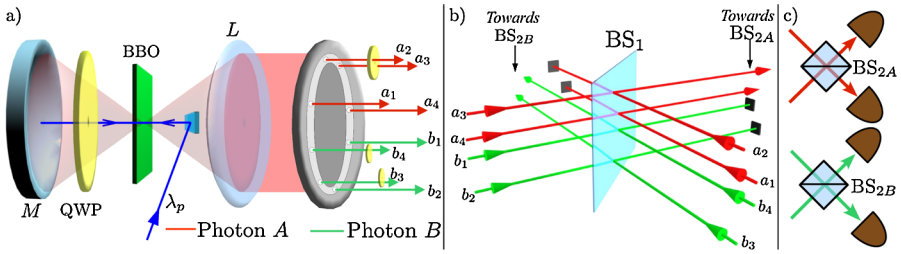

FIG. 2 (color online). Generation of the six-qubit linear cluster state. (a) Scheme of the entangled two-photon six-qubit parametric source: a UV laser beam (wavelength λ_p) impinges on the Type I BBO crystal after reflection on a small mirror. The polarization entangled state $(|H\rangle|H\rangle - |V\rangle|V\rangle)/\sqrt{2}$ arises from the superposition of the degenerate emission cones of the crystal. Basic elements of the source are: (i) A spherical mirror (M), reflecting both the parametric radiation and the pump beam, whose micrometric displacement enables phase control between the $|H\rangle|H\rangle$ and $|V\rangle|V\rangle$ events. (ii) A quarter wave plate (WP), located between mirror M and BBO, performing the $|H\rangle|H\rangle \rightarrow |V\rangle|V\rangle$ transformation on the left cone. (iii) A positive lens L, transforming the conical parametric emission of the crystal into a cylindrical one. Four pairs of correlated longitudinal modes $a_i - b_i$ ($i = 1, \ldots, 4$) are selected by an eight-hole screen. One half WP oriented at 45° intercepting modes a_2, a_3 and two half WPs oriented at 0° intercepting b_3, b_4 determine the transformation from $|\widetilde{\mathrm{HE}}_6\rangle$ to $|\widetilde{\mathrm{LC}}_6\rangle$. (b) Spatial superposition between the left (ℓ) and right (r) modes on the common 50/50 beam splitter BS$_1$. ℓ modes a_1, a_2 (b_3, b_4) are respectively matched with r modes a_4, a_3 (b_2, b_1) on the A (B) side. Temporal indistinguishability is obtained by setting to zero the path delay between the right and the left modes. (c) Spatial superposition between the internal I (a_2, a_3, b_2, b_3) and external E (a_1, a_4, b_1, b_4) modes is performed on BS$_{2A}$ and BS$_{2B}$ for the A and B photon, respectively. Independent adjustment of time delay between the A and B modes coming out of BS$_1$ determines interference between the modes. After BS$_1$, only the A (B) modes contribute to the interference on BS$_{2A}$ (BS$_{2B}$), while the others modes are intercepted by beam stops.

where $|\phi^{\pm}\rangle_{\pi} = \frac{1}{\sqrt{2}}(|HH\rangle_{AB} \pm |VV\rangle_{AB})$ and $|\psi^{\pm}\rangle_{\pi} = \frac{1}{\sqrt{2}}(|HV\rangle_{AB} \pm |VH\rangle_{AB})$ are the standard polarization Bell states.

The transformation from the hyperentangled state to the cluster state was carried out by two wave plates intercepting the $|\widetilde{\mathrm{HE}}_6\rangle$'s output modes. Precisely, since qubits 1 (E/I) and 2 (H/V) are encoded in photon A, the CX_{12} gate was obtained by applying a half wave plate (WP) oriented at 45° on the internal A modes (a_2 and a_3 in Fig. 2). Equivalently, the CZ_{65} was obtained by inserting a half WP oriented at 0° on the left B modes (b_3 and b_4). In the actual experiment, we used one WP intercepting both a_2 and a_3 modes, while one WP was used for the b_3 mode and one for the b_4 mode [see Fig. 2(a)].

The experimental setup sketched in Figs. 2(b) and 2(c) allows the simultaneous measurement of three single-qubit compatible observables for each particle. It is given by two chained interferometers whose core elements are given by three symmetric (50/50) beam splitters BS_1, BS_{2A}, and BS_{2B}. In BS_1, the four ℓ modes are made indistinguishable from the corresponding r modes both in space and time, while I and E modes belonging to the A (B) side are matched on BS_{2A} (BS_{2B}). Two pairs of single photon detectors detect the output modes A or B, while polarization entanglement is measured by four polarization analyzers (not shown in the figure), one for each detector. Nearly 500 coincidences per second were detected, which is 4 orders of magnitude larger than the rate of the six-photon linear cluster state [16].

Fidelity.—We measured the fidelity of our preparation by measuring the 64 stabilizers $\tilde{s}_i$ of the $|\widetilde{\mathrm{LC}}_6\rangle$, i.e., all the products of the generators $\tilde{g}_i$. We obtained [25]

$$F = \frac{1}{64}\sum_{i=1}^{64}\langle\tilde{s}_i\rangle = 0.6350 \pm 0.0008, \tag{6}$$

which constitutes an improvement of 7% with respect to the best previous fidelity for six-qubit graph states with six particles [15,16]. The fidelity value is limited by imperfections in phase and polarization settings, such as the two controlled operations (CX and CZ), and mainly by nonperfect mode matching on the three beam splitters (BSs). Note that the measurements on the second momentum (I/E qubit) are naturally affected by imperfections of the first momentum setup. Using single mode fibers combined with integrated quantum optical circuits in the experimental setup would allow to largely restore the state fidelity [26]. Other DOFs, such as time-energy and orbital angular momentum, could be adopted to increase the number of qubits. However, this imposes the use of optical components of high quality to preserve the fidelity.

Entanglement witness.—We tested whether or not the created state has genuine six-qubit entanglement (i.e., inexplicable by five or less qubit entanglement). For that purpose, we measured an entanglement witness specifically designed [27] to detect genuine six-qubit entanglement around the $|\widetilde{\mathrm{LC}}_6\rangle$,

$$\mathcal{W}_F = \mathbb{1} - 2|\widetilde{\mathrm{LC}}_6\rangle\langle\widetilde{\mathrm{LC}}_6| = \mathbb{1} - \frac{1}{32}\sum_{i=1}^{64}\tilde{s}_i, \tag{7}$$

where $\mathbb{1}$ is the identity operator. There is entanglement whenever

$$\langle\mathcal{W}_F\rangle = 1 - 2F < 0. \tag{8}$$

We obtained,

$$\mathcal{W}_F = -0.270 \pm 0.002, \tag{9}$$

which is negative by 135 standard deviations and thus proves the existence of a genuine six-qubit entanglement.

Quantum nonlocality.—The specific state we have created is the only distribution of six qubits between two particles whose perfect correlations have the same nonlocality as those of the six-qubit Greenberger-Horne-Zeilinger state [6] and, instead of requiring six separated carriers to show nonlocality, it only requires two [5]. In any local theory in which all the single-qubit Pauli observables can be regarded as elements of reality in the sense of EPR [21], the following Bell inequality [6] must hold:

$$\mathcal{B} \leq 4 \equiv B_{\mathrm{LHV}}, \tag{10}$$

where

$$\mathcal{B} = |\tilde{g}_1(\mathbb{1} + \tilde{g}_2)(\mathbb{1} + \tilde{g}_3)(\mathbb{1} + \tilde{g}_4)(\mathbb{1} + \tilde{g}_5)\tilde{g}_6|. \tag{11}$$

This inequality is the optimal one to detect nonlocality even when the $|\widetilde{\mathrm{LC}}_6\rangle$ has a maximum amount of white noise [6]. EPR's assumption is that single-qubit observables on photon A (B) are elements of reality (i.e., have preassigned outcomes) when their outcomes can be predicted with probability 1 from measurements on photon B (A). However, in our experiment, the single-qubit observables on photon A (B) in the inequality (10) can be predicted from measurements on photon B (A) with probabilities ranging from 0.78 to 0.94. Therefore, we need to relax EPR's assumption and assume that single-qubit Pauli observables are elements of reality if they can be predicted with probability higher than 0.77. For example, if $\langle X_3 Z_5 X_6\rangle = 1 - \epsilon$, with $0 \leq \epsilon \ll 1$, then a fraction ϵ $(1 - \epsilon)$ of the pairs are uncorrelated (perfectly correlated). Therefore, the outcome of X_3 in photon A can be correctly predicted from the outcome of $Z_5 X_6$ in photon B with probability 1 for the the correlated pairs and with probability $\frac{1}{2}$ for the uncorrelated pairs. Thus the outcome of X_3 can be predicted with probability $1(1 - \epsilon) + \frac{1}{2}\epsilon = 1 - \frac{\epsilon}{2}$.

We tested the Bell inequality (10) and obtained

$$\mathcal{B}_{\mathrm{exp}} = 7.018 \pm 0.028, \tag{12}$$

equivalent to a degree of nonlocality $\mathcal{D} = \frac{\mathcal{B}_{\mathrm{exp}}}{B_{\mathrm{LHV}}}$ of 1.7545 ± 0.0070, which is a considerable improvement compared to previous violations of Bell inequalities only

involving perfect correlations and using four-qubit states: $(2.59 \pm 0.08)/2 = 1.29$ [12], $(2.73 \pm 0.12)/2 = 1.36$ [13], $(3.4145 \pm 0.0095)/2 = 1.70$ [17] and $(2.50 \pm 0.04)/2 = 1.25$ [28]. A higher value of $\mathcal{D}$ has been reached for a Bell inequality not involving perfect correlations [10,29,30]. To our knowledge, the result of Eq. (12) represents the first nonlocality test with a six-qubit graph state. The fact that we have obtained a higher degree of nonlocality than with simpler systems is an experimental confirmation that quantum nonlocality can increase as the complexity of the system grows in spite of the decrease of the fidelity [3].

Persistency of entanglement.—Linear cluster states are particular entangled states that, when some qubits are lost, still present some entanglement and nonlocality [1]. Here we can check that, by tracing qubits 3 and 6 or, alternatively, qubits 1 and 4, the remaining four qubits are still entangled and violate a Bell inequality. Indeed, we observed the violation of the two following Bell inequalities:

$$\beta \leq 2, \tag{13a}$$

$$\beta' \leq 2, \tag{13b}$$

where,

$$\beta = |\tilde{g}_1(\mathbb{1} + \tilde{g}_2)(\mathbb{1} + \tilde{g}_4)|, \tag{14a}$$

$$\beta' = |(\mathbb{1} + \tilde{g}_3)(\mathbb{1} + \tilde{g}_5)\tilde{g}_6|. \tag{14b}$$

The first is a 2-2-0-2-1-0-setting Bell inequality (i.e., it only involves measurements on qubits 1, 2, 4, and 5); the second is a 0-1-2-0-2-2-setting Bell inequality (i.e., it only involves measurements on qubits 2, 3, 5, and 6). We tested these two Bell inequalities, obtaining

$$\beta_{\text{exp}} = 2.325 \pm 0.014, \tag{15a}$$

$$\beta'_{\text{exp}} = 2.881 \pm 0.012. \tag{15b}$$

These results correspond, respectively, to a violation of 23 and 73 standard deviations. The fact that the violation in (15a) is lower than that in (15b) is due to the critical E/I mode matching occurring on BS_{2A}, and BS_{2B}. We attribute this to the angular divergence of the selected modes that enhances their transverse size in the measurement setup.

Conclusions.—In this Letter we have presented the first experimental demonstration of a six-qubit linear cluster state built on a two-photon triple entangled state. An entanglement witness has been measured for this state and its persistency of entanglement and quantum nonlocality properties have been characterized in detail. Cluster states built on two photons and more DOFs present both advantages and disadvantages with respect to multiphoton cluster states. On one side, no more than few pairs of photons at a time are created by spontaneous parametric down conversion, due to the probabilistic nature of this process; then, multiphoton detection is seriously affected by the limited quantum efficiencies of detectors; finally, an entangled state built on a large number of particles is more affected by decoherence because of the increased difficulty of making photons indistinguishable. On the other side, increasing the number of DOFs implies an exponential requirement of resources, for instance, 2^N **k** modes per photon must be selected within the emission cone to encode N qubits in each photon. Despite that, working with a limited number of DOFs (up to four) is still more convenient than increasing the number of photon pairs. Hence a hybrid approach (i.e., multi-DOF/multiphoton states) can be conceived in a medium-term time scale to overcome the structural limitations in generation or detection of quantum photon states.

The authors thank O. Gühne for useful conversations. This work was supported by the Spanish MCI Project No. FIS2008-05596 and the Junta de Andalucía Excellence Project No. P06-FQM-02243 and by Finanziamento Ateneo 08 Sapienza Universitá di Roma.

*http://quantumoptics.phys.uniroma1.it/

[1] R. Raussendorf and H. J. Briegel, Phys. Rev. Lett. **86**, 5188 (2001); H. J. Briegel and R. Raussendorf, *ibid.* **86**, 910 (2001).
[2] M. Hein *et al.*, Phys. Rev. A **69**, 062311 (2004).
[3] N. D. Mermin, Phys. Rev. Lett. **65**, 1838 (1990).
[4] O. Gühne *et al.*, Phys. Rev. Lett. **95**, 120405 (2005).
[5] A. Cabello and P. Moreno, Phys. Rev. Lett. **99**, 220402 (2007).
[6] A. Cabello *et al.*, Phys. Rev. A **77**, 062106 (2008).
[7] D. Schlingemann and R. F. Werner, Phys. Rev. A **65**, 012308 (2001).
[8] W. Dür and H. J. Briegel, Phys. Rev. Lett. **92**, 180403 (2004).
[9] C. A. Sackett *et al.*, Nature (London) **404**, 256 (2000).
[10] Z. Zhao *et al.*, Phys. Rev. Lett. **91**, 180401 (2003).
[11] P. Walther *et al.*, Nature (London) **434**, 169 (2005).
[12] P. Walther *et al.*, Phys. Rev. Lett. **95**, 020403 (2005).
[13] N. Kiesel *et al.*, Phys. Rev. Lett. **95**, 210502 (2005).
[14] R. Prevedel *et al.*, Nature (London) **445**, 65 (2007).
[15] D. Leibfried *et al.*, Nature (London) **438**, 639 (2005).
[16] C.-Y. Lu *et al.*, Nature Phys. **3**, 91 (2007).
[17] G. Vallone *et al.*, Phys. Rev. Lett. **98**, 180502 (2007).
[18] K. Chen *et al.*, Phys. Rev. Lett. **99**, 120503 (2007).
[19] G. Vallone *et al.*, Phys. Rev. Lett. **100**, 160502 (2008).
[20] W.-B. Gao *et al.*, arXiv:0809.4277.
[21] A. Einstein *et al.*, Phys. Rev. **47**, 777 (1935).
[22] M. Barbieri *et al.*, Phys. Rev. A **72**, 052110 (2005).
[23] G. Vallone *et al.*, Phys. Rev. A **79**, 030301(R) (2009).
[24] A. Rossi *et al.*, Phys. Rev. Lett. **102**, 153902 (2009).
[25] See EPAPS Document No. E-PRLTAO-103-003944 for a table of stabilizer measurements. For more information on EPAPS, see http://www.aip.org/pubservs/epaps.html.
[26] A. Politi *et al.*, Science **320**, 646 (2008).
[27] G. Tóth and O. Gühne, Phys. Rev. Lett. **94**, 060501 (2005).
[28] X.-Q. Zhou *et al.*, Phys. Rev. A **78**, 012112 (2008).
[29] M. Ardehali, Phys. Rev. A **46**, 5375 (1992).
[30] O. Gühne and A. Cabello, Phys. Rev. A **77**, 032108 (2008).